

Y. Wang, L. Xiang, J. Zhang and X. Ge, “Connectivity Analysis for Large-Scale Intelligent Reflecting Surface Aided mmWave Cellular Networks,” accepted for presentation in *IEEE International Symposium on Personal, Indoor and Mobile Radio Communications (PIMRC)*, Sep. 2022.

©2022 IEEE. Personal use of this material is permitted. However, permission to reprint/republish this material for advertising or promotional purposes or for creating new collective works for resale or redistribution to servers or lists, or to reuse any copyrighted component of this works must be obtained from the IEEE.

Connectivity Analysis for Large-Scale Intelligent Reflecting Surface Aided mmWave Cellular Networks

Yufei Wang¹, Lin Xiang², Jing Zhang¹, and Xiaohu Ge¹

¹School of Electronic Information and Communications, Huazhong University of Science and Technology

²Communications Engineering Lab, Technische Universität Darmstadt

Emails: {yufeiwang,zhangjing,xhge}@hust.edu.cn, l.xiang@nt.tu-darmstadt.de

Abstract—This paper presents a stochastic geometry framework for modeling and evaluating the connectivity of uplink transmission in a large-scale intelligent reflecting surface (IRS) assisted millimeter-wave (mmWave) communication network, where the uplink user equipments (UEs) attempt to communicate with the nearest base stations (BSs) either without or with the help of an IRS. We propose a novel elliptical geometry model, which can effectively capture the impact of IRS location and orientation, as well as incident/reflection angle on mmWave signal propagation, while, at the same time, significantly simplifying the analysis of the system performance. Employing the elliptical geometry model, the approximate reflection probability of IRS as well as its upper and lower bounds are derived in closed form. Based on these results, we further analyze the successful connection probability of uplink UEs for IRS-assisted mmWave cellular networks. Our results show that compared with conventional direct UE-to-BS communication without IRS, indirect communication with the aid of IRS exhibits a slower decaying in the connection probability as the communication distance increases, as the latter can significantly increase the connection probability for cell-edge UEs. Moreover, for mmWave BSs with small receiving power thresholds, the deployment of IRS can effectively mitigate the impact of blockages to improve mmWave signal propagation.

Index Terms—Intelligent Reflecting Surfaces (IRS), Blockage, Stochastic Geometry.

I. INTRODUCTION

Millimeter-wave (mmWave) communications usually require strong line-of-sight (LoS) channel conditions to mitigate the large propagation loss of mmWave signals. However, mmWave communications in urban areas can severely suffer from blockages caused by e.g. buildings and trees [1]. To address this challenge, application of intelligent reconfigurable surfaces (IRSs) for enhanced mmWave communications has recently attracted significant interest in both academia and industry [2], [3]. Thereby, through tuning the phase shifts of the metasurface units, the IRS enables to scatter/reflect mmWave signals towards desired directions, which can increase the likelihood of establishing LoS mmWave communications between base stations (BSs) and user equipments (UEs). Moreover, due to its passive nature, IRS consumes much less energy than conventional relay nodes. Further, the IRSs can be easily deployed on the facade of buildings for extending mmWave cellular coverage to urban communication hot spots.

The work is supported by the National Natural Science Foundation of China under Grant U2001210, Hubei Provincial Science and Technology Department under Grant 2021BAA009. The work of L. Xiang has been funded by the LOEWE initiative (Hesse, Germany) within the emergenCITY center and the BMBF project Open6GHub under grant 16KISK014.

In [4], the authors considered joint optimization of power allocation, user association and beamforming for maximizing the sum rate of an IRS-assisted mmWave communication system. In [5], the authors considered joint optimization of BS transmit precoding and IRS phase shift for maximizing the received signal power. However, the aforementioned works have only considered IRS-aided mmWave communications in small-scale networks with a limited number of nodes (UEs, BSs, and IRSs) and/or blockages. Extending the research to large-scale IRS-aided mmWave networks is crucially needed for evaluating the performance of IRS-aided mmWave communications and gaining insights for future practical deployment.

Motivated by the aforementioned research need, in this paper, we consider performance analysis of large-scale IRS-aided mmWave networks in urban areas using the stochastic geometry theory, which takes into account large-scale randomly distributed nodes (UEs, BSs, and IRSs) and blockages. As has been shown in the literature [6]–[10], the stochastic geometry tool can accurately capture the characteristics of BS deployment and user distributions in practical cellular networks, while still enabling tractable analyses of the network performance. To our knowledge, stochastic geometry has not been employed for analyzing large-scale IRS-aided mmWave cellular networks except in [11], where the authors analyzed the signal-to-interference-ratio (SIR) of mmWave communication and the coverage probability. However, the results in [11] ignored the impact of blockages on mmWave signal propagation, which are not applicable to urban mmWave cellular networks. On the other hand, although modeling and analyses of IRS-aided cellular networks using stochastic geometry have also been considered for non-orthogonal multiple access (NOMA) networks in [12], [13] and traditional cellular networks in [14], they have not considered mmWave communications. In fact, the approaches in [11]–[14] cannot be applied for our problem in a straightforward manner, as this would be overly complicated. In particular, for the considered IRS-aided mmWave communication in presence of blockages, the system performance depends jointly on the incident and reflection/scattering angles of mmWave signals at the IRSs. The latter is difficult to characterize using the existing approaches in [11]–[14].

To tackle these challenges, in this paper, we propose a novel elliptic geometry model for analyzing the scattering/reflection mechanism of large-scale IRS-aided mmWave uplink transmissions. By utilizing the geometric properties of the proposed model, the impact of the incidence and reflection angles of the

mmWave signal on the connectivity of the IRS-aided mmWave communications can be captured analytically with greatly simplified effort. This further facilitates a tractable analysis of the connection probability for uplink UEs without and with the aid of IRS. Our derivations are validated by Monte Carlo simulations. Both the numerical and the simulation results reveal that the deployment of IRS can significantly improve the connection probability of cell-edge mmWave UEs and, for networks with small receiving power threshold, IRS can effectively mitigate the impact of blockages on mmWave signal propagations.

The remainder of this paper is organized as follows. In Sec. II, the system model of the considered IRS aided uplink mmWave transmission is presented. The reflection probability in IRS aided mmWave signal transmission and the total connection probability of a typical UE are analyzed in Sec. III. The numerical and simulation results are presented in Sec. IV, where the impact of communication distance and receiving power threshold is investigated. Finally, Sec. V concludes the paper.

II. SYSTEM MODEL

A. Network and Blockage Model

As shown in Fig. 1, we consider uplink communication in an IRS aided mmWave network in an urban area, where the BSs are distributed over the whole R^2 plane to provide seamless access service to the UEs. Let y_i and x_j be the locations of BS i and UE j , respectively. The locations of the BSs and the UEs, denoted by $\Phi_{BS} = \{y_i; i = 1, 2, 3 \dots\}$ and $\Phi_u = \{x_j; j = 1, 2, 3 \dots\}$, are assumed to follow homogeneous Poisson Point Processes (PPPs) with densities λ_{BS} and λ_u , respectively. We assume that Φ_u is independent of Φ_{BS} . Moreover, λ_u is large enough so that each mmWave BS serves exactly one UE in any given resource block and no BSs are idle [15].

As mmWave signals have weak diffraction and penetration capabilities, buildings lying between the UEs and BSs can significantly degrade the mmWave signal propagation. We assume that, for any UE-to-BS link whose LoS path is blocked by buildings in between, the power received at the BS is negligible [14]. To enhance mmWave signal propagation in the considered urban environment, IRSs are deployed on $\mu \in [0, 1]$ fraction of the buildings, where each building can mount at most one IRS. We assume that the lengths and widths of the buildings follow independent uniform distributions in the range of $(\mathbb{E}[L] - l_0, \mathbb{E}[L] + l_0)$ and $(\mathbb{E}[W] - w_0, \mathbb{E}[W] + w_0)$, respectively. $\mathbb{E}[L]$ and $\mathbb{E}[W]$ are the expected length and width of the buildings, respectively. In this paper, we assume $\mathbb{E}[L]$, $\mathbb{E}[W]$, l_0 , and w_0 are given, cf. Table I in Sec. IV. Moreover, the center locations of the buildings, denoted by Φ_b , follows a PPP with density λ_b , independent of Φ_{BS} and Φ_u . Consequently, the locations of IRSs, denoted by Φ_R , follow a PPP with density $\lambda_R = \mu\lambda_b$.

B. UE-to-BS Association

The UEs transmit signals at a given output power P_{\max} . The UEs and the BSs employ antenna arrays with M_u and M_b antenna elements, respectively. However, each UE has only

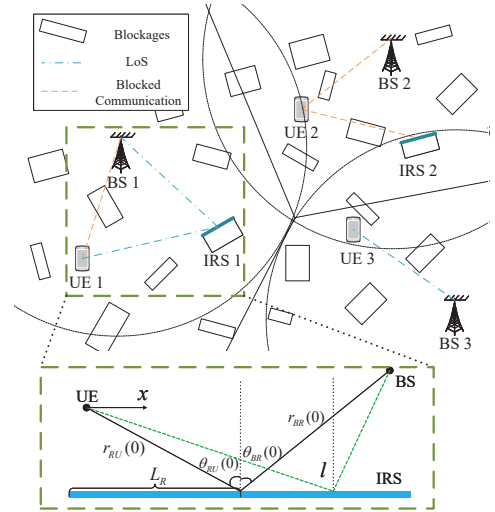


Fig. 1. Network model of IRS aided mmWave communications in an urban area.

one radio frequency (RF) chain, such that only one data stream is sent for communicating with its intended BS. Consequently, the antenna arrays at the UE and its intended BS are mainly used for beamforming purpose, so as to mitigate the propagation loss of mmWave signals [16]. Moreover, we assume that each UE attempts to associate with the nearest BS in its communication range such that, if successful, the path loss of mmWave signal propagation is further minimized. Considering a typical UE and its associated BS located at x and y^s , we have $y^s = \arg \min_{y \in \Phi_{BS}} \|y - x\|$, where $\|\cdot\|$ denotes the Euclidean distance.

Due to blockages caused by the buildings, a portion of the UEs may not be able to connect to their nearest BS for direct LoS (DLoS) communication. Then, these UEs will attempt an indirect LoS (ILoS) transmission, i.e., to communicate with its nearest BS via an IRS. To this end, the IRS having the minimal effective path loss over the end-to-end UE-to-IRS-to-BS link is chosen. That is, the IRS located at t^s is selected if and only if $t^s = \arg \min_{t \in \Phi_R} \delta\{t\} (\|y^s - t\|^\alpha \cdot \|t - x\|^\alpha)$, where $\delta\{t\} = 1$ if the IRS located at t can establish an ILoS connection from the UE to its associated BS and otherwise $\delta\{t\} = \infty$. We note that the defined association scheme is not capacity-achieving but is considered in order to facilitate a tractable analysis of the network connectivity.

As a UE performing DLoS transmission would always experiences a shorter signal propagation path than when performing ILoS communication, the UEs will employ DLoS communication with a high priority, i.e., they will attempt ILoS communication only after the attempt of DLoS communication to the nearest BS fails.

C. Effective Channel Model for DLoS and ILoS Transmissions

We consider small-scale fading and path loss for modeling the mmWave channel [16]. In particular, for the BS at y^s , its received signal power from the UE located at x is given by $P_e \triangleq P_x |h_{x,y^s}|^2 C_s L_{x,y^s}$, where P_x is the transmit power of the UE and C_s is the propagation path loss at a reference distance

of 1 m. $|h_{x,y^s}|$ denotes the *effective* small-scale fading gain for mmWave communication from x to y^s , which is a scalar since we are only interested in the received power P_e of beamformed mmWave signals. To capture the LoS dominant mmWave propagation channels, we assume independent Nakagami fading for each link, i.e., $|h_{x,y^s}|^2 \sim \Gamma(N_s, 1)$ is Gamma distributed with unit mean power, where N_s is the effective fading parameter after considering transmit and receiver beamforming over the underlying mmWave multiple-input multiple-output channel [16]. Note that h_{x,y^s} can be obtained by employing maximum ratio combining on independent Nakagami fading paths [17]. Finally, L_{x,y^s} is the path loss for mmWave communication from x to y^s . For example, $L_{x,y^s} = \|y^s - x\|^{-\alpha}$ for DLoS transmission, where $\alpha \in [2, 4]$ is the path loss exponent.

To further characterize L_{x,y^s} for ILoS transmission, let us first consider mmWave signal transmission from the typical UE to its associated BS via scattering/reflection at an IRS of length $2L_R$ centered at $(x_R(0), y_R(0))$, cf. Fig. 1. Any point on the IRS with distance $l \in [-L_R, L_R]$ from the center of the IRS has a coordinate given as $(x_R(l), y_R(l)) = (x_R(0) + l \cos \theta_R(l), y_R(0) + l \sin \theta_R(l))$, where $\theta_R(l) \in (-\pi, \pi]$ is an auxiliary angle parameter. Moreover, $r_Q(l)$ and $\theta_Q(l)$, $Q \in \{BR, RU\}$, denote the distances and incident/reflection angles associated with the BS-to-IRS and IRS-to-UE links at $(x_R(l), y_R(l))$. Assume $r_Q \gg 2L_R$. Then the propagation distance from the UE to point $(x_R(l), y_R(l))$ on IRS can be approximated as $r_Q(l) \approx r_Q(0) + ql \sin(\theta_Q(0))$, where $q = 1$ if $Q = BR$, and $q = -1$ if $Q = RU$. Following a similar approach as [13], the path loss for ILoS transmission is given by $L_{x,y^s} = M \left| \int_{-L_R}^{+L_R} \Psi(l) \exp(-j \frac{2\pi}{\lambda} \Omega(l)) dl \right|^2$, where λ is the wave length of the considered mmWave signal and M is the number of metasurface strips deployed on an IRS. $\Psi(l) = \frac{\cos(\theta_{BR}(l)) + \cos(\theta_{RU}(l))}{8\pi \sqrt{r_{BR}(l)r_{RU}(l)}}$ and $\Omega(l) = r_{BR}(l) + r_{RU}(l) - \Theta(l)$ denote the amplitude and phase (or precisely overall propagation distance) of mmWave signals received at the BS via scattering/reflection at $(x_R(l), y_R(l))$ of the IRS, respectively, where $\Theta(l)$ is the phase shift of metasurface unit at point $(x_R(l), y_R(l))$ of the IRS. In this paper, we set $\Theta(l) = (\sin(\theta_{BR}(0)) - \sin(\theta_{RU}(0)))l + \frac{\phi_0 \lambda}{2\pi}$, where $\phi_0 \in [0, 2\pi)$ is a fixed phase shift [13]. Thereby, substitute $\Theta(x)$ into $\Psi(x)$, we have $\Psi(l) = r_{BR}(0) + r_{RU}(0) - \frac{\phi_0 \lambda}{2\pi}$, i.e., the mmWave signals scattered/reflected at different points of the IRS are cophase and can be coherently superimposed (provided the mmWave signals are coherently combined at the BS). Consequently, for ILoS transmission, we have [13]

$$L_{x,y^s} \approx C_t^2 (r_{BR}(0)r_{RU}(0))^{-\alpha}, \quad (1)$$

where $C_t = \frac{ML_R}{4\pi} (\cos(\theta_{BR}(0)) + \cos(\theta_{RU}(0)))$.

Now, generalizing the results in (1) to the selected IRS located at t^s , the large-scale propagation L_{x,y^s} can be described as

$$L_{x,y^s} = \begin{cases} \|y^s - x\|^{-\alpha}, & \text{for DLoS scheme,} \\ C_{t^s}^2 (r_{x,t^s} r_{t^s,y^s})^{-\alpha}, & \text{for ILoS scheme.} \end{cases} \quad (2)$$

where r_{t^s,y^s} and r_{x,t^s} denote the distances from the BS at y^s and the UE at x to the center of the IRS at t^s , respectively. θ_{t^s,y^s} and θ_{x,t^s} denote the reflection and the incident

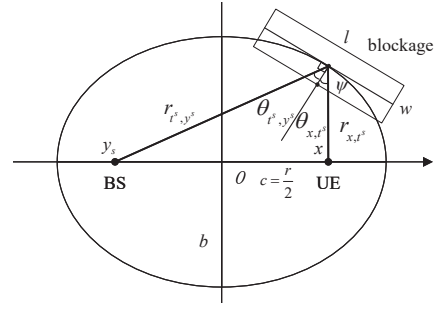


Fig. 2. Proposed elliptic geometry model for characterizing IRS scattering. angles at the center of the IRS, respectively. And $C_{t^s} = \frac{ML_R}{4\pi} (\cos(\theta_{x,t^s}) + \cos(\theta_{t^s,y^s}))$.

D. System Performance Metric and Proposed Elliptic Geometry Model

To characterize the impact of IRS on mmWave communications, we will analyze the connectivity of the considered IRS-assisted mmWave cellular network, which is defined as

$$\mathbb{P}_c = \int_0^\infty (\mathbb{P}_{\text{DLoS}}(r) \mathbb{P}_{D|r}\{P_e > P_{th}\} + (1 - \mathbb{P}_{\text{DLoS}}(r)) \mathbb{P}_{\text{ILoS}}(r) \mathbb{P}_{I|r}\{P_e > P_{th}\}) f_R(r) dr. \quad (3)$$

In (3), $\mathbb{P}_{\text{DLoS}}(r)$ and $\mathbb{P}_{\text{ILoS}}(r)$ are the probabilities that the typical UE located at a distance of r from its associated BS can perform DLoS and ILoS transmissions, respectively. $\mathbb{P}_{D|r}\{P_e > P_{th}\}$ and $\mathbb{P}_{I|r}\{P_e > P_{th}\}$ are the probabilities that the signal power received at the associated BS, P_e , exceeds the threshold P_{th} for establishing DLoS and ILoS communications, respectively. Finally, $f_R(\cdot)$ is the probability density function (PDF) of the distance between the typical UE and its associated BS, denoted by R . And we have $f_R(r) = 2\pi \lambda_{BS} r e^{-\lambda_{BS} \pi r^2}$, which is obtained from the void probability of PPP following [18].

However, analyzing ILoS transmission in (3) is particularly challenging. This is because, for ILoS transmission, L_{x,y^s} depends jointly on parameters θ_{x,t^s} , θ_{t^s,y^s} , r_{x,t^s} and r_{t^s,y^s} , which are functions of the locations of the BS, the UE, and the IRS. Representing these parameters in polar coordinates results in complex expressions and complicates the derivation process. To facilitate a tractable analysis, we further propose an elliptic geometry model for analyzing θ_{x,t^s} , θ_{t^s,y^s} , r_{x,t^s} and r_{t^s,y^s} in the considered stochastic geometry framework. In particular, let the origin O be located in the middle of the UE and the BS. Moreover, define an ellipse with focal length $c = \frac{r}{2}$ such that the BS and the UE coincide with the focal points of the ellipse, cf. Fig. 2. Consequently, an arbitrary point in the R^2 plane, denoted as (x, y) , can be alternatively described in a parametric form as $x = \sqrt{b^2 + c^2} \cos \theta$ and $y = b \sin \theta$, where b and θ are the length of the minor axis of the ellipse and an auxiliary angle parameter, respectively. Meanwhile, for the associated BS at y^s and the IRS at t , we have $r_{x,t} = \sqrt{b^2 + c^2} - c \cos \theta$ and $r_{t,y^s} = \sqrt{b^2 + c^2} + c \cos \theta$. As will be shown in Sec. III, with the proposed model, convenient geometric properties of ellipse can be exploited to simplify the analyses of IRS-aided mmWave

communications. For example, when the UE and its associated BS are in the far field of the IRS, we have $\theta_{x,t} + \theta_{t,y^s} = \psi$, where $\psi = \arcsin \frac{2bc \sin \theta}{b^2 + c^2 \sin^2 \theta}$ is the angle between the UE-to-IRS link and the BS-to-IRS link, namely the focal vertex angle, cf. Fig. 2.

III. UPLINK PERFORMANCE ANALYSIS

A. Analyses of DLoS and ILoS Probabilities

In this section, we first analyze the probabilities of associating with BSs at a distance of r from the typical UE before establishing DLoS and ILoS transmissions, i.e. $\mathbb{P}_{\text{DLoS}}(r)$ and $\mathbb{P}_{\text{ILoS}}(r)$, respectively. Based on the derived results, the impact of the BS receiving threshold on UE-to-BS association will be further analyzed in Section III-B. For the DLoS scheme, the following lemma reveals that the probability of association, $\mathbb{P}_{\text{DLoS}}(r)$, decreases exponentially with distance r , as the number of blockages grows with r .

Lemma 1. *For a typical mmWave UE, the probability of associating to the BS at a distance of r away for DLoS transmission is given as*

$$\mathbb{P}_{\text{DLoS}}(r) = \exp(-\beta r - p), \quad (4)$$

where $\beta = \frac{2}{\pi} \lambda_b (\mathbb{E}[L] + \mathbb{E}[W])$ and $p = \lambda_b \mathbb{E}[L] \mathbb{E}[W]$ characterize the average impact of the blockage sizes on mmWave signal propagation.

Proof: The proof follows from [19] and is ignored herein for saving page space. ■

On the other hand, when the typical UE employs ILoS transmission, $\mathbb{P}_{\text{ILoS}}(r)$ is given as the probability of having at least one IRS for enabling an indirect LoS path from the typical user to the associated BS at a distance of r away [14]. Taking into account the sizes of the blockages, we introduce a protection distance of $r_{\min} = \sqrt{(\mathbb{E}[W] + w_0)^2 + (\mathbb{E}[L] + l_0)^2}$, such that the distance from the center of a blockage to the UE or the BS should exceed r_{\min} , i.e. all UEs and BSs are located away from the blockages. Meanwhile, for an IRS located on the ellipse, we require both the IRS-to-BS and IRS-to-UE distances to exceed r_{\min} . This equivalently sets $\sqrt{b^2 + c^2} - c > r_{\min}$, i.e., $b > \sqrt{r_{\min}^2 + r \cdot r_{\min}} \triangleq b_1$. Finally, using the proposed elliptical model, $\mathbb{P}_{\text{ILoS}}(r)$ is derived in closed form in the following theorem.

Theorem 1. *Assume that the distance between the typical UE and its associated BS is r . The probability of having at least one IRS to reflect the mmWave signals from the UE to the BS is given as*

$$\mathbb{P}_{\text{ILoS}}(r) = 1 - \exp\left(-\frac{4\lambda_R}{w_2 - w_1} I(r)\right), \quad (5)$$

where $I(r) = \int_{w_1}^{w_2} \int_0^{\pi/2} \int_{b_1}^{\infty} \mathcal{E}(b) \mathcal{C}(r, b, \theta, w) \mathcal{J}(b, \theta) db d\theta dw$ characterizes the average number of IRSs that can reflect the mmWave signals from the UE to the BS located at a distance of r away with $\mathcal{E}(b) = e^{-2(p + \beta \sqrt{b^2 + c^2})}$, $w_1 = \mathbb{E}[W] - w_0$, and $w_2 = \mathbb{E}[W] + w_0$. Moreover, $\mathcal{C}(r, b, \theta, w) = \frac{1}{2\pi} \left(\pi - \sin^{-1} \frac{w}{2r_{x,t^s}} - \sin^{-1} \frac{w}{2r_{t^s,y^s}} - \psi \right)$ is the probability that an IRS located at (b, θ) with width w is properly oriented

such that both the typical UE and its associated BS are in front of the IRS, where $\sin^{-1} \frac{w}{2r_{x,t^s}}$ and $\sin^{-1} \frac{w}{2r_{t^s,y^s}}$ are the angles caused by the width of the blockage and the lengths of UE-to-IRS link or IRS-to-BS link, respectively. Finally, $\mathcal{J}(b, \theta) = \frac{b^2 + c^2 \sin^2 \theta}{\sqrt{b^2 + c^2}}$ is due to coordinate transformation using the proposed elliptic geometry model.

Proof: Please refer to Appendix A. ■

However, $\mathbb{P}_{\text{ILoS}}(r)$ in (5) involves a sophisticated triple-integral term $I(r)$, which is inconvenient to evaluate. In the following, we further simplify the results by deriving an approximate value of $I(r)$ as well as its upper and lower bounds.

Proposition 1. *The triple-integral term $I(r)$ can be approximated as*

$$I(r) \approx I_0(r) \triangleq \int_{b_1}^{\infty} \mathcal{E}(b) \left((w_2 - w_1) \mathcal{X}_a(b) - \frac{\pi}{4} (w_2^2 - w_1^2) \right) db, \quad (6)$$

where $\mathcal{X}_a(b) = \int_0^{\pi/2} \left(\pi - \arcsin \frac{2bc \sin \theta}{b^2 + c^2 \sin^2 \theta} \right) \mathcal{J}(b, \theta) d\theta$. Moreover, $\mathcal{X}_a(b)$ is bounded as $\mathcal{X}_l(b) < \mathcal{X}_a(b) < \mathcal{X}_u(b)$, where $\mathcal{X}_l(b) = \frac{\pi}{\sqrt{b^2 + c^2}} \left(\arctan \frac{b}{c} \left(b^2 + \frac{c^2}{2} \right) - 1 \right)$ and $\mathcal{X}_u(b) = \frac{\pi \left(\frac{\pi}{2} b^2 + c^2 \right) - 2bc}{\sqrt{b^2 + c^2}}$.

Proof: For $\theta \rightarrow 0$, we have $\arcsin \theta \approx \theta$. Moreover, when $w \ll r_{x,t^s}$ and $w \ll r_{t^s,y^s}$, we have

$$\begin{aligned} \sin^{-1} \frac{w}{2r_{x,t^s}} + \sin^{-1} \frac{w}{2r_{t^s,y^s}} &\approx \frac{w}{2r_{x,t^s}} + \frac{w}{2r_{t^s,y^s}} \\ &= \frac{w(r_{t^s,y^s} + r_{x,t^s})}{2r_{t^s,y^s} r_{x,t^s}} = \frac{w\sqrt{b^2 + c^2}}{b^2 + c^2 \sin^2 \theta}. \end{aligned} \quad (7)$$

Substituting these approximations into $I(r)$, (6) can be obtained. Moreover, as $\theta \in (0, \pi/2]$, we have $\arcsin \theta > \theta > \sin \theta$ and

$$\mathcal{X}_a(b) < \int_0^{\frac{\pi}{2}} \left(\pi - \frac{2bc \sin \theta}{b^2 + c^2 \sin^2 \theta} \right) \mathcal{J}(b, \theta) d\theta = \mathcal{X}_u(b). \quad (8)$$

Finally, exploiting the property of ellipse, we have $\psi = 2 \arctan \frac{c \sin \theta}{b}$ and

$$\begin{aligned} \mathcal{X}_a(b) &= \frac{1}{\sqrt{b^2 + c^2}} \left(\pi \left(\arctan \frac{b}{c} \left(b^2 + \frac{c^2}{2} \right) - 1 \right) \right. \\ &\quad \left. + \int_0^{\frac{\pi}{2}} \left(\left(b^2 + \frac{c^2}{2} \right) \theta - \frac{c^2 \sin 2\theta}{4} \right) \frac{2bc \cos \theta}{b^2 + c^2 \sin^2 \theta} d\theta \right) \\ &\stackrel{(a)}{>} \frac{1}{\sqrt{b^2 + c^2}} \pi \left(\arctan \frac{b}{c} \left(b^2 + \frac{c^2}{2} \right) - 1 \right) = \mathcal{X}_l(b), \end{aligned} \quad (9)$$

where (a) is due to $\theta > \frac{\sin(2\theta)}{2}$ for $\theta > 0$. This completes the proof. ■

Fig. 3 shows the reflection probability $\mathbb{P}_{\text{ILoS}}(r)$, its approximate value and upper/lower bounds versus the UE-to-BS distance, r . From Fig. 3, we observe that the approximation value is in good agreement with the exact value of $I(r)$. Moreover, the reflection probability $\mathbb{P}_{\text{ILoS}}(r)$ decreases monotonically with r . This is because, as r increases, the UE-to-IRS and IRS-to-BS links have larger lengths and, hence, are more likely to be blocked. Further, $\mathbb{P}_{\text{ILoS}}(r)$ decreases the fastest for $r \in [200 \text{ m}, 600 \text{ m}]$. This is because, in addition to the increased

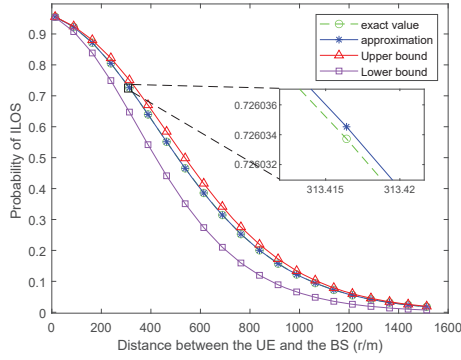


Fig. 3. Exact value of $\mathbb{P}_{\text{ILoS}}(r)$ versus its approximate value as well as upper and lower bounds.

lengths and blockages of the UE-to-IRS and IRS-to-BS links, the likelihood of having a properly oriented IRS reduces, as r increases in this range.

B. Connectivity Analysis

In Sec. III-A, the reflection probability $\mathbb{P}_{\text{ILoS}}(r)$ has characterized the impact of the IRS orientation on establishing an ILoS signal path. In this section, we further analyze the impact of signal incidence and reflection angles at the IRS on the received signal power at the BS. To this end, we first analyze the path loss of the IRS-assisted communication link using the proposed elliptic geometry model. Based on the obtained results, the successful connection probabilities $\mathbb{P}_{D|r}\{P_e > P_{th}\}$ and $\mathbb{P}_{I|r}\{P_e > P_{th}\}$ are further derived.

1) *Path Loss of IRS Reflection*: For the ILoS transmission via IRS, the connection probability $\mathbb{P}_{I|r}\{P_e > P_{th}\}$ depends jointly on the incident and reflection angles of mmWave signals, as well as the length, position and orientation of the IRS, as revealed in the following lemma.

Lemma 2. Let \mathcal{O} denote the random orientation of a typical IRS. Then the expected path loss of the IRS located at (b, θ) , averaged with respect to \mathcal{O} , is given as

$$\mathbb{E}_{\mathcal{O}}[L_{x,y^s}] = M^2 \frac{L_R^2}{16\pi^2} \frac{b^2}{(b^2 + c^2 \sin^2 \theta)^{1+\alpha}}. \quad (10)$$

Proof: Please refer to Appendix B. ■

2) *Connection Probability*: Based on Lemma 2, the conditional connection probabilities of DLoS and ILoS transmissions, given that the UE is associated with the BS at a distance of r , are given in the following theorem.

Theorem 2. Let (B, Θ) denote the random location of the IRS. The probabilities of successfully performing DLoS and ILoS transmissions by the uplink UEs, when the UE-to-BS distance is r , are given as

$$\mathbb{P}_{D|r}\{P_e > P_{th}\} = 1 - \left(1 - \exp\left(-\frac{\eta_s P_{th} r^\alpha}{P_x M_b M_u C_s}\right)\right)^{N_s}, \quad (11)$$

$$\mathbb{P}_{I|r}\{P_e > P_{th}\} = 1 - \int_0^\infty f_{L_R}(L_R) \cdot$$

$$\mathbb{E}_{B,\Theta} \left[\left(1 - \exp\left(-\frac{16\pi^2 \eta_s P_{th} (b^2 + c^2 \sin^2 \theta)^{1+\alpha}}{M L_R^2 P_{\max} M_b M_u C_s b^2}\right)\right)^{N_s} \right] dL_R,$$

respectively, where $f_{L_R}(L_R)$ is the PDF of the IRS length.

TABLE I
PARAMETERS SETTINGS [14], [19]

Parameter	Default Value	Parameter	Default Value
λ_{BS}	$10^{-5}/\text{m}^2$	M	5
λ_b	$5 \times 10^{-4}/\text{m}^2$	P_x	1 W
λ_u	$3 \times 10^{-4}/\text{m}^2$	μ	0.2
$\mathbb{E}[L]$	10 m	$\mathbb{E}[W]$	5 m
l_0	2 m	w_0	1 m
α	3	C_s	$1/4\pi^2$
N_s	3	L_R	4 m
M_b	18	M_u	10

Proof: Let H and \mathcal{L} denote the random small-scale fading and IRS length, respectively. According to (2), we have

$$\begin{aligned} & \mathbb{P}_{D|r}\{P_e > P_{th}\} \\ &= \mathbb{P}\left\{M_b M_u P_x C_s |h_{x,y^s}|^2 r^{-\alpha} \geq P_{th}\right\} \\ &= 1 - \mathbb{P}\left\{|h_{x,y^s}|^2 < \frac{P_{th} r^\alpha}{P_x M_b M_u C_s}\right\} \\ &\stackrel{(b)}{\approx} 1 - \left(1 - \exp\left(-\frac{\eta_s P_{th} r^\alpha}{P_x M_b M_u C_s}\right)\right)^{N_s}, \end{aligned} \quad (12)$$

and

$$\begin{aligned} & \mathbb{P}_{I|r}\{P_e > P_{th}\} \\ &\stackrel{(c)}{\approx} \mathbb{P}_{H,B,\Theta,\mathcal{L}}\{P_x M_b M_u C_s |h_{x,y^s}|^2 \mathbb{E}_{\mathcal{O}}[L_{x,y^s}(r)] \geq P_{th}\} \\ &= 1 - \mathbb{E}_{B,\Theta,\mathcal{L}}\left\{\mathbb{P}_H\left[|h_{x,y^s}|^2 < \frac{16\pi^2 P_{th}}{M^2 L_R^2 P_x M_b M_u C_s}\right.\right. \\ &\quad \left.\left.\frac{1}{b^2} (b^2 + c^2 \sin^2 \theta)^{1+\alpha}\right]\right\} \\ &\stackrel{(d)}{\approx} 1 - \mathbb{E}_{B,\Theta,\mathcal{L}}\left\{\left[1 - \exp\left(-\eta_s \frac{16\pi^2 P_{th}}{M^2 L_R^2 P_x M_b M_u C_s}\right.\right.\right. \\ &\quad \left.\left.\frac{1}{b^2} (b^2 + c^2 \sin^2 \theta)^{1+\alpha}\right)\right]^{N_s}\right\}, \end{aligned} \quad (13)$$

where (b) and (d) follows from [16, Lemma 6] with $\eta_s = N_s(N_s!)^{-\frac{1}{N_s}}$. (c) is due to the fact that the location and the orientation of IRSs are independent. Note that for any function of random variables B and Θ , denoted as $f(B, \Theta)$, its expectation is given as

$$\mathbb{E}_{B,\Theta}[f(B, \Theta)] = \int_0^{+\infty} \int_0^{2\pi} f_{B,\Theta}(b, \theta) f(b, \theta) d\theta db \quad (14)$$

where $f_{B,\Theta}(b, \theta) = \frac{\lambda_R(2b^2+c^2)}{2\sqrt{b^2+c^2}} \exp(-\pi\lambda_R b\sqrt{b^2+c^2})$ [18]. ■

Finally, by substituting (4), (5), (11) and (14) into (3), the total connectivity probability \mathbb{P}_c in (3) is obtained.

IV. NUMERICAL RESULTS

In this section, the derived analytical results are validated using Monte Carlo simulations, where the location of the buildings and RIS are randomly generated according to PPP. Moreover, we evaluate the impact of the receiving signal thresholds of BSs and the densities of blockages on the system performance. Unless otherwise specified, the simulation parameters are set according to Table I. For convenience, in the following, we refer to $\mathbb{P}_d(r) = \mathbb{P}_{\text{DLoS}}(r)\mathbb{P}_{D|r}\{P_e > P_{th}\}$ and $\mathbb{P}_i(r) =$

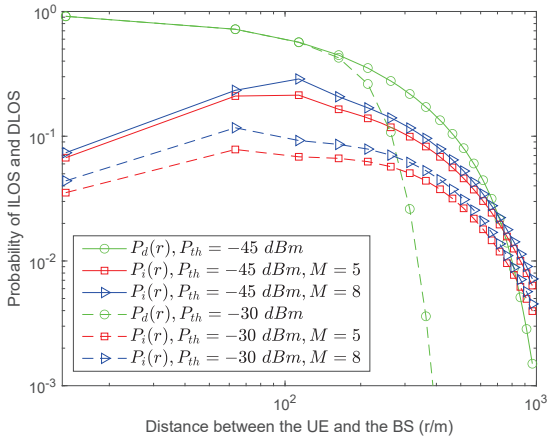


Fig. 4. Connection probability of DLoS and ILoS transmissions versus the UE-to-BS distance, r .

$(1 - \mathbb{P}_{\text{DLoS}}(r)) \mathbb{P}_{\text{ILoS}}(r) \mathbb{P}_{I|r}\{P_e > P_{th}\}$ as the effective connection probabilities of DLoS and ILoS transmissions when the UE-to-BS distance is r .

Fig. 4 shows $\mathbb{P}_d(r)$ and $\mathbb{P}_i(r)$ as functions of the UE-to-BS distance r for different transmission schemes. From Fig. 4 we observe that $\mathbb{P}_d(r)$ monotonically decreases with the UE-to-BS distance, r . This is because, as r increases, the UE-to-BS link is more likely to be blocked and, at the same time, experiences a larger path loss. However, the connection probability of ILoS transmission increases with r in the small regime, but decreases with r in the large regime. That is, there exists an optimal UE-to-BS distance for implementing ILoS communication via IRS. This is because, unlike $\mathbb{P}_d(r)$, the term $(1 - \mathbb{P}_{\text{DLoS}}(r))$ in $\mathbb{P}_i(r)$ increases with r . From Fig. 4 we also observe that, when the UE is far away from the BSs, $\mathbb{P}_d(r)$ decreases much faster with the UE-to-BS distance than $\mathbb{P}_i(r)$. This is because the probability of having DLoS links, $\mathbb{P}_{\text{DLoS}}(r)$, decreases exponentially with r , cf. Lemma 1. However, for ILoS scheme, the mmWave signals can propagate over multiple pairs of shorter paths and are more likely to find an unblocked ILoS path, cf. Theorem 1. Hence, $\mathbb{P}_i(r)$ decreases with r more slowly than $\mathbb{P}_d(r)$, even though the ILoS communication experiences a larger path loss. This result implies that the deployment of IRS in mmWave cellular networks can significantly improve the connection probability of cell-edge UEs.

Finally, Fig. 5 shows $\mathbb{P}_D \triangleq \int_0^\infty \mathbb{P}_d(r) f_R(r) dr$, $\mathbb{P}_I \triangleq \int_0^\infty \mathbb{P}_i(r) f_R(r) dr$, and $\mathbb{P}_c = \mathbb{P}_D + \mathbb{P}_I$ as functions of the threshold of received signal power at the BSs for different densities of buildings, where $\lambda_{b1} = 5 \times 10^{-4}/\text{m}^2$ and $\lambda_{b2} = 2.5 \times 10^{-4}/\text{m}^2$. From Fig. 5 we observe that, as the receiving power threshold decreases, the probability of implementing DLoS communication, \mathbb{P}_D , saturates as blockages have a dominant impact on the connectivity in the small power threshold regime. However, as the density of blockages increases, both \mathbb{P}_D and \mathbb{P}_I decrease monotonically due to the increased blockages. From Fig. 5 we also observe that, for small receiving power thresholds, the total connection probability, \mathbb{P}_c , is close to 1, where most of the UEs can

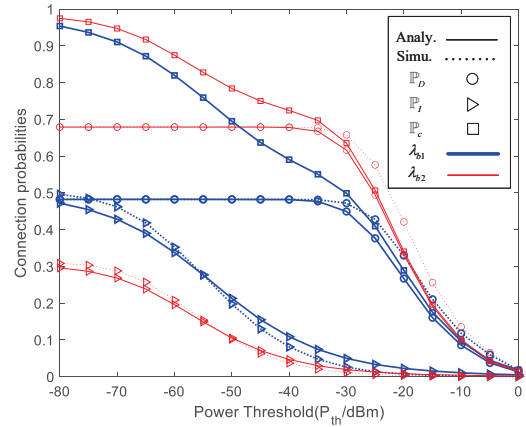


Fig. 5. Probabilities of DLoS and ILoS transmissions, and total connection probability versus the threshold of received signal power.

successfully connect with the BSs. This result implies that the deployment of IRSs in mmWave networks is most advantageous if the receiving power threshold is sufficiently small.

V. CONCLUSION

In this paper, the successful connection probability of a large-scale IRS-assisted urban mmWave cellular network was analyzed for uplink UEs performing DLoS and ILoS transmissions. We introduced a novel elliptic geometry model to facilitate a tractable analysis of the reflection probability via the IRS. Moreover, simpler approximate expressions of the reflection probability as well as the upper and lower bounds were provided. Based on the reflection probability, the total connection probability for uplink communication with and without the IRS was further derived. Our analytical results were validated by Monte Carlo simulations, both of which further showed that the deployment of IRS can significantly enhance the connectivity of the considered mmWave network, particularly for cell-edge UEs and BSs with sufficiently small received power threshold. In this paper, PPPs are used to model the spatial locations of BSs, UEs and buildings. Extending the proposed elliptic geometry model to more sophisticated spatial distributions of BSs, UEs, and buildings, such as thinning PPP [20] and Binomial Point Process (BPP) [21], is an interesting work for future consideration.

APPENDIX A PROOF OF THEOREM 1

The typical UE can perform ILoS communication if and only if at least one IRS is properly located and oriented whereby the IRS has (i) a LoS connection with the user, (ii) a LoS connection with the BS and (iii) a proper orientation such that both the UE and the BS are located in front of the IRS. We have

$$\begin{aligned} \mathbb{P}_{\text{ILoS}}(r) &= 1 - \mathbb{P}(\mathcal{N} = 0) \\ &\stackrel{(a)}{=} 1 - \exp\left(-\lambda_R \iiint_{\Omega} \mathbb{P}'_I(r) \mathcal{J}(b, \theta) db \, d\theta \, dw\right), \end{aligned} \quad (15)$$

where \mathcal{N} denotes the number of IRSs satisfying conditions (i)–(iii), (a) is based on the void probability of PPP, Ω is the integral region for (b, θ, w) , and $\mathbb{P}'_I(r)$ is the probability that an IRS can fulfill conditions (i)–(iii) for given UE-to-BS distance of r .

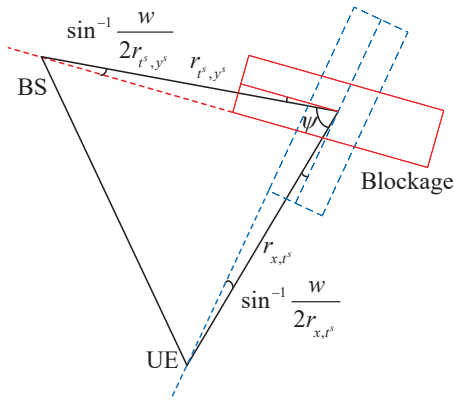


Fig. 6. Two extreme cases that can support reflection.

Fig. 6 shows two extreme cases where condition (iii) is fulfilled [14]. Accordingly, $\mathbb{P}'_I(r)$ can be calculated as

$$\begin{aligned} \mathbb{P}'_I(r) &= e^{-p-\beta r_{x,t}} e^{-p-\beta r_{t,y^s}} \mathcal{C}(r, b, \theta, w) \\ &\stackrel{(b)}{=} e^{-2p-2\beta\sqrt{b^2+c^2}} \mathcal{C}(r, b, \theta, w) \end{aligned} \quad (16)$$

where (b) is due to $r_{x,t} + r_{t,y^s} = 2\sqrt{b^2+c^2}$ for any t on an ellipse. $e^{-p-\beta r_{x,t}}$, $e^{-p-\beta r_{t,y^s}}$ and $\mathcal{C}(r, b, \theta, w) = \frac{1}{2\pi} (\pi - \sin^{-1} \frac{w}{2r_{x,t}} - \sin^{-1} \frac{w}{2r_{t,y^s}} - \psi)$ are the probabilities of events (i), (ii) and (iii), respectively. Based on (16), the density of IRSs satisfying conditions (i)–(iii) is $\mathbb{P}'_I(r)\lambda_R$.

Finally, substituting (16) into (15), we can obtain (5), which completes the proof.

APPENDIX B PROOF OF LEMMA 2

Based on (2), we have

$$\mathbb{E}_{\mathcal{O}} [L_{x,y^s}(r)] = \mathbb{E}_{\mathcal{O}} [C_{t^s}^2] (r_{x,t^s} r_{t^s,y^s})^{-\alpha}, \quad (17)$$

where $C_{t^s} = \frac{ML}{4\pi} (\cos(\theta_{x,t^s}) + \cos(\theta_{t^s,y^s}))$. Moreover, we have

$$\begin{aligned} &\mathbb{E}_{\mathcal{O}} [(\cos \theta_{x,t^s} + \cos \theta_{t^s,y^s})^2] \\ &\stackrel{(c)}{=} \frac{2}{\pi} \int_0^{\frac{\pi}{2}} (\cos^2 \theta_{x,t^s} + \cos^2 \theta_{t^s,y^s} + 2 \cos \theta_{x,t^s} \cos \theta_{t^s,y^s}) d\theta_{x,t^s} \\ &= \frac{1 + \cos \psi}{2} \frac{\pi - \psi + \sin \psi}{\pi} \stackrel{(d)}{\approx} \frac{1 + \cos \psi}{2}, \end{aligned} \quad (18)$$

where (c) is due to the fact that θ_{x,t^s} is uniformly distributed in $[-\frac{\pi}{2} + \psi, \psi]$ [13]. (d) follows from $\sin \psi \approx \psi$, when ψ is small. When ψ is close to π , (d) also holds as $1 + \cos \psi \approx 0$ and $(\sin \psi - \psi)(1 + \cos \psi) \approx 0$.

Substituting (18) to (2), we have

$$\begin{aligned} \mathbb{E}_{\mathcal{O}} [L_{x,y^s}] &\stackrel{(e)}{=} \frac{M^2 L^2}{16\pi^2} \frac{b^2}{r_{x,t^s} r_{t^s,y^s}} (r_{x,t^s} r_{t^s,y^s})^{-\alpha_i} \\ &= \frac{M^2 L^2}{16\pi^2} \frac{b^2}{(b^2 + c^2 \sin^2 \theta)^{1+\alpha_i}}, \end{aligned} \quad (19)$$

where (e) follows from $r_{x,t} r_{t,y^s} = \frac{2b^2}{1+\cos \psi}$ for any t located on an ellipse. This completes the proof.

REFERENCES

- [1] J. G. Andrews, T. Bai, M. N. Kulkarni, and et al., "Modeling and analyzing millimeter wave cellular systems," *IEEE Trans. Commun.*, vol. 65, no. 1, pp. 403–430, Oct. 2017.
- [2] S. Gong, X. Lu, D. T. Hoang, and et al., "Toward smart wireless communications via intelligent reflecting surfaces: A contemporary survey," *IEEE Commun. Surveys Tuts.*, vol. 22, no. 4, pp. 2283–2314, Jun. 2020.
- [3] Q. Wu and R. Zhang, "Towards smart and reconfigurable environment: Intelligent reflecting surface aided wireless network," *IEEE Commun. Mag.*, vol. 58, no. 1, pp. 106–112, Nov. 2020.
- [4] P. Wang, J. Fang, X. Yuan, Z. Chen, and H. Li, "Intelligent reflecting surface-assisted millimeter wave communications: Joint active and passive precoding design," *IEEE Trans. Veh. Technol.*, vol. 69, no. 12, pp. 14 960–14 973, Oct. 2020.
- [5] D. Zhao, H. Lu, Y. Wang, H. Sun, and Y. Gui, "Joint power allocation and user association optimization for IRS-assisted mmWave systems," *IEEE Trans. Wireless Commun.*, vol. 21, no. 1, pp. 577–590, Jul. 2022.
- [6] X. Ge, J. Ye, Y. Yang, and Q. Li, "User mobility evaluation for small cell networks based on individual mobility model," *IEEE J. Sel. Areas Commun.*, vol. 34, no. 3, pp. 528–541, 2016.
- [7] X. Ge, B. Yang, J. Ye, G. Mao, C.-X. Wang, and T. Han, "Spatial spectrum and energy efficiency of random cellular networks," *IEEE Trans. Commun.*, vol. 63, no. 3, pp. 1019–1030, 2015.
- [8] Y. Zhong, T. Q. Quek, and X. Ge, "Heterogeneous cellular networks with spatio-temporal traffic: Delay analysis and scheduling," *IEEE J. Sel. Areas Commun.*, vol. 35, no. 6, pp. 1373–1386, 2017.
- [9] J. Zhang, L. Xiang, D. W. K. Ng, M. Jo, and M. Chen, "Energy efficiency evaluation of multi-tier cellular uplink transmission under maximum power constraint," *IEEE Wireless Commun.*, vol. 16, no. 11, pp. 7092–7107, 2017.
- [10] J. Zhang, J. Han, L. Xiang, D. W. K. Ng, M. Chen, and M. Jo, "On the performance of dual-mode uplink transmission: Connection probability versus energy efficiency," *IEEE Trans. Veh. Technol.*, vol. 69, no. 10, pp. 11 152–11 168, 2020.
- [11] M. Nemat, J. Park, and J. Choi, "RIS-assisted coverage enhancement in millimeter-wave cellular networks," *IEEE Access*, vol. 8, pp. 188 171–188 185, Oct. 2020.
- [12] T. Hou, Y. Liu, Z. Song, X. Sun, Y. Chen, and L. Hanzo, "Reconfigurable intelligent surface aided NOMA networks," *IEEE J. Sel. Areas Commun.*, vol. 38, no. 11, pp. 2575–2588, Jul. 2020.
- [13] C. Zhang, W. Yi, Y. Liu, and et al., "Reconfigurable intelligent surfaces aided multi-cell NOMA networks: A stochastic geometry model," *IEEE Trans. Commun.*, vol. 70, no. 2, pp. 951–966, Nov. 2022.
- [14] M. A. Kishk and M.-S. Alouini, "Exploiting randomly located blockages for large-scale deployment of intelligent surfaces," *IEEE J. Sel. Areas Commun.*, vol. 39, no. 4, pp. 1043–1056, Aug. 2021.
- [15] A. AlAmmouri, J. G. Andrews, and F. Baccelli, "SINR and throughput of dense cellular networks with stretched exponential path loss," *IEEE Trans. Wireless Commun.*, vol. 17, no. 2, pp. 1147–1160, Nov. 2018.
- [16] T. Bai and R. W. Heath, "Coverage and rate analysis for millimeter-wave cellular networks," *IEEE Trans. Wireless Commun.*, vol. 14, no. 2, pp. 1100–1114, Oct. 2015.
- [17] J. Zhang, X. Ge, Z. Li, G. Mao, and Y. Yang, "Analysis of the uplink maximum achievable rate with location-dependent intercell signal interference factors based on linear Wyner model," *IEEE Trans. Veh. Technol.*, vol. 62, no. 9, pp. 4615–4628, Jun. 2013.
- [18] S. N. Chiu, D. Stoyan, W. S. Kendall, and J. Mecke, *Stochastic Geometry and Its Applications*. U.K.: Wiley, 2013.
- [19] T. Bai, R. Vaze, and R. W. Heath, "Analysis of blockage effects on urban cellular networks," *IEEE Trans. Wireless Commun.*, vol. 13, no. 9, pp. 5070–5083, Jun. 2014.
- [20] Y. Hmamouche, M. Benjillali, and S. Saoudi, "Fresnel line-of-sight probability with applications in airborne platform-assisted communications," *IEEE Trans. Veh. Technol.*, vol. 71, no. 5, pp. 5060–5072, 2022.
- [21] T. Shafique, H. Tabassum, and E. Hossain, "Stochastic geometry analysis of assisted downlink cellular networks," *IEEE Trans. Commun.*, vol. 70, no. 2, pp. 1442–1456, 2022.